High-throughput investigation of osteoblast response to polymer crystallinity: influence of nanometer-scale roughness on proliferation ☆

Newell R. Washburn[a],*, Kenneth M. Yamada[b], Carl G. Simon Jr.[a],
Scott B. Kennedy[a], Eric J. Amis[a]

[a] Polymers Division, National Institute of Standards and Technology, Gaithersburg, MD 20899, USA
[b] National Institute of Dental and Craniofacial Research, National Institutes of Health, Bethesda, MD 20892, USA

Abstract

A high-throughput method for analyzing cellular response to crystallinity in a polymer material is presented. Variations in crystallinity lead to changes in surface roughness on nanometer length scales, and it is shown that cells are exquisitely sensitive to these changes. Gradients of polymer crystallinity were fabricated on films of poly(L-lactic acid) using a gradient in annealing temperature. The resultant morphologies were characterized using an atomic force microscope. Root-mean-square (rms) roughness values ranging from 0.5 to 13 nm were created on a single sample. MC3T3-E1 osteoblastic cells were cultured for 1, 3 and 5 d, and the number of cells was measured using automated fluorescence microscopy. It is shown that the rate of proliferation on the smooth regions of the films is much greater than that on the rough regions, and a monotonic variation in rate is observed as a function of roughness. The critical rms roughness, above which a statistically significant reduction in rate of proliferation occurs, was approximately 1.1 nm. Fluorescence microscopy measurements on immunostained cells indicate there is no significant change in cell area, the number or type of adhesions formed, or the degree of actin polymerization. Results from enzyme-linked immunofluorescence assays indicated that there was no detectable change in adhesion protein accessibility, suggesting the cells directly respond to substrate topography. The use of the gradient library approach yielded the functional dependence of cell proliferation on nanometer-scale roughness and gave a sensitive estimate of the critical roughness for which a decrease in proliferation is observed.

1. Introduction

The interaction of cells with materials is a highly complicated subject, but one that is important both in cell biology and a broad range of medical applications. The response of cells to structured surfaces suggests they are sensitive to substrate topography [1–4], but it has been difficult to perform systematic investigations of cellular response to this material variable. Investigating these interactions can be further complicated by variations in cell population [5] and culture conditions. To address these issues we have been developing high-throughput methods for investigating cell–material interactions [6]. The approach is based on a gradient library technique where a single sample is created with a systematic variation in material parameters along one or two orthogonal directions so that the cellular response across the sample maps out the influence of this parameter. For the one-dimensional libraries, adherent cells along the direction orthogonal to the gradient experience essentially identical conditions, and the average response may be measured in a statistically

☆ Certain equipment and instruments or materials are identified in the paper to adequately specify the experimental details. Such identification does not imply recommendation by the National Institute of Standards and Technology, nor does it imply the materials are necessarily the best available for the purpose. According to ISO 31-8, the term "molecular weight" has been replaced by "relative molecular mass", M_r. The conventional notation, rather than the ISO notation, has been employed for this publication.

*Corresponding author.

E-mail address: newell.washburn@nist.gov (N.R. Washburn).

relevant manner. In this preliminary study we have investigated the proliferation of osteoblastic MC3T3-E1 cells to a fundamental material variable: crystallinity.

There have been reports of cellular response to crystalline materials but to our knowledge, no one has performed a systematic study of the influence of nanometer-scale roughness on adherent cells. Park and Griffith [7] performed a study of spheroid formation by hepatocytes and proliferation of fibroblasts on poly(L-lactic acid) (PLLA) substrates, the results of which suggest cells proliferate more slowly on crystalline vs. smooth PLLA. However, their conclusions were slightly complicated by the use of glancing-angle X-ray diffraction to characterize the substrates, a technique that is well suited for assessing the degree of crystallinity but does not directly yield information on topography. Mikos et al. [8] investigated tissue ingrowth through porous scaffolds composed of semicrystalline or amorphous poly(lactic acid) that were implanted in rat mesentary. For the samples that were not soaked in saline solution prior to implantation, there was a nearly twofold reduction in percent tissue in-growth through the crystalline scaffolds after 10 d as compared to the amorphous scaffolds. Their results also suggest qualitatively that cell proliferation is adversely affected by substrate roughness, but the functional dependence was not established.

In this work we investigated the sensitivity of osteoblastic MC3T3-E1 cells to changes in nanometer-scale structure. Single samples having variations in degree of crystallinity that lead to changes in roughness from less than 1 to 13 nm were prepared and the proliferation measured as a function of position across the samples. Experiments probing the concentration or conformation of adherent attachment proteins were also performed to probe whether the observed effects were truly due to substrate topography. Immunofluorescence staining was done to investigate some possible mechanisms of the observed effects.

2. Materials and methods

2.1. Materials

PLLA was obtained from Polysciences. Solutions were prepared by dissolving PLLA in chloroform (Fisher), and insoluble contaminants that could act as nucleation sites for crystallization were removed using a 0.2 μm filter. The substrate used for polymer-film coating was a polished silicon wafer (Wafer World, Inc.) that was exposed to UV radiation for 5 min to create a hydroxide coating. Following UV treatment, the wafer was immersed in 2% solution (by mass fraction) of chlorodimethyloctylsilane (Aldrich) in

toluene (Fisher) for 30 min, gently rinsed in toluene and placed under vacuum at 150°C for 2 h. This creates a hydrophobic surface to which PLLA will adhere when the substrate is immersed in aqueous media.

2.2. Gradient library preparation

Solutions of 3% PLLA in chloroform (by mass fraction) were prepared and cast onto a silanized silicon wafer using a custom-built flow-coater [9] and kept under vacuum at room temperature for 10 d to remove residual solvent. Film thicknesses ranged from 250 to 350 nm as measured using a Filmetrics interferometer. The samples were cut into $6 \text{ cm} \times 1.5 \text{ cm}$ coupons and annealed on a custom-built temperature gradient stage [9] with the limits of the stage held at 44°C and 100°C. The linearity of the temperature gradient was verified using an array of thermocouples [10], and the homogeneity of the resultant crystallinity gradient was verified using optical microscopy.

2.3. Substrate topography measurements

Tapping-mode atomic force microscopy (AFM) was performed with a Digital Instruments Dimension 3100 Nanoscope III. The root-mean-square (rms) roughness was calculated for each image using the instrument software. The standard uncertainty is denoted by the error bars, which represent the standard deviation over multiple measurements.

2.4. Cell culture

Established protocols for the culture and passage of MC3T3-E1 cells were followed [11]. Cells were obtained from Riken Cell Bank (Hirosaka, Japan) and cultured in flasks (75 cm^2 surface area) at 37°C in a fully humidified atmosphere at 5% CO_2 (volume fraction) in α modification of Eagle's Minimum Essential Medium (Biowhittaker, Inc., Walkersville, MD) supplemented with 5% (volume fraction) fetal bovine serum (GIBCO, Rockville, MD) and kanamycin sulfate (Sigma, Inc., St. Louis, MO). Media was changed twice weekly and cultures were passaged with 2.5 g/l trypsin (mass fraction 0.25%) and 1 mmol/l EDTA (GIBCO, Rockville, MD) once per week. Cultures of 90% confluent MC3T3-E1 cells were trypsinized, washed and suspended in fresh media. One hundred thousand cells diluted into 4 ml of media were added to wells containing the gradient libraries and given 10 min to settle before the samples were moved to the incubator. When performing the proliferation experiments it was crucial to seed the cells evenly and give them time to form preliminary attachments before transporting the flask to the incubator; even slight vibrations were capable of

producing clumps of cells in the center of the sample that would lead to significant variations in the numbers of cells at each position. Samples were cultured for 1, 3 or 5 d without changing medium and fixed using 4% formaldehyde (by mass fraction) (Aldrich) in phosphate-buffered saline.

2.5. Automated fluorescence microscopy

Cells were stained with 4,6-diamidino-2-phenylindole hydrochloride (DAPI) for cell-counting and counter-stained with phalloidin:Texas Red (Molecular Probes) for measuring degree of actin polymerization per cell or Texas Red:maleimide (Molecular Probes) for measuring area per cell and mounted on a microscope slide using Vectashield mounting fluid (Vector). Automated fluorescence microscopy was performed with a Leica DMR 1200 Inverted Microscope equipped with a computer-controlled translation stage. The samples were imaged in a (10×10) grid at a magnification of $10 \times$. These spatially correlated counts were used as a measure of proliferation as a function of position. The data at 1 d were also used to verify that the cell seeding resulted in a homogeneous coating of cells, both parallel and perpendicular to the gradient.

2.6. Focal adhesion imaging

Focal adhesions were stained using a paxillin antibody (Transduction Laboratories) and species-specific secondary antibodies (Jackson Immunoresearch) and imaged with a Zeiss laser scanning confocal microscope at $63 \times$.

2.7. Enzyme-linked immunofluorescence assay (ELISA)

Variations in the amount or conformation of sub-strate-bound attachment proteins were investigated with an Amplex ELISA kit (Molecular Probes) on discreet, homogeneous samples. Human fibronectin was obtained from Chemicon International. Mouse anti-human fibronectin developed by Schoen et al. [12] was obtained from the Developmental Studies Hybridoma Bank developed under the auspices of the NICHD and maintained by the University of Iowa, Department of Biological Sciences, Iowa City, IA 52242. Mouse anti-human vitronectin 615.2C3.23 (Innovative Research) was used to stain for bovine vitronectin from serum and found to have good cross-species reactivity. Absorbance measurements were performed at 580 nm, with a background reading due to non-specific binding of 1200. The standard uncertainty is denoted by the error bars, which represent the standard deviation over multiple measurements.

3. Results and discussion

3.1. Library preparation and characterization

The crystallinity libraries are made of PLLA having a gradient in degree of crystallinity created by annealing on a temperature gradient. This method has been shown to be of use in investigating the crystallization kinetics of other polymers such as isotactic polystyrene [10]. Polymer crystallization occurs via the formation of a critical nucleus from which crystallites grow at a linear rate that is determined by the transport properties of the polymer. The rate of crystallite nucleation I^* is determined by the Gibbs free energy of crystallization ΔG^*, which decreases sharply below the melting temperature T_m, and the Gibbs free energy of activation ΔG_η, which increases as the glass transition temperature T_g is approached from above, I^* is modeled as having the following functional form [13]:

$$I^* = (Nk_B T/h)\exp\big[-(\Delta G^* + \Delta G_\eta)/k_B T\big], \qquad (1)$$

where N is the number of uncrystallized elements able to participate in nucleation, $k_B T$ is the thermal energy, and h is Planck's constant. This equation predicts a roughly parabolic rate of crystallite nucleation, shown in Fig. 1, which is due to competition between the increased stability of nuclei and the decreased polymer mobility as the temperature is lowered. Fig. 1 was generated using a reaction rate theory expression for ΔG^*, a WLF-type expression for ΔG_η [13] and experimental parameters for T_g, T_m, surface tensions, heat of fusion, and density of PLLA [14]. The temperature range used in the gradients $(44-100^\circ\text{C}$ or $317-373\,\text{K})$ corresponds to the region of the curve where the rate of nucleation is predicted to increase monotonically with increasing temperature, which was observed in our experiments. Limiting the
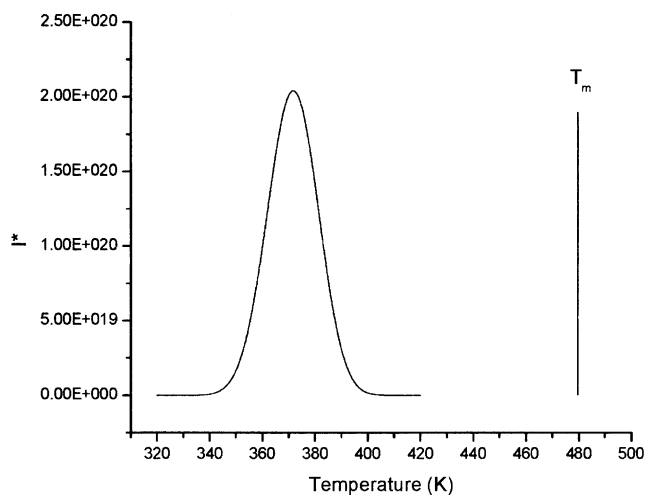
Fig. 1. Plot of PLLA nucleation rate in units of number of crystallized monomers/s/mol as a function of temperature as predicted by Eq. (1) in the text. The vertical line represents the melting temperature of T_m of bulk PLLA.

time for which crystallization can occur freezes the film into various stages of nucleation and growth, leading to a gradient in substrate roughness.

The topography as a function of film position was measured using an AFM, and the representative images are shown in Fig. 2(a)–(e). In Fig. 2(a) can be seen the amorphous surface with only isolated surface contaminants and an rms roughness of (0.54 ± 0.17) nm. Roughening due to incipient nucleation is observed in Fig. 2(b), leading to topographic feature heights approximately (5 ± 1) nm and an rms roughness of (1.05 ± 0.21) nm. In Fig. 2(c), nuclei are observed with heights ranging from 5 to 20 nm and an rms roughness of (3.84 ± 0.92) nm. In Fig. 2(d), the nucleation density is quite high and the crystallites are poorly formed, suggesting the rate of nucleation competes effectively with that of crystal growth. The maximum rms roughness in this regime is (13.00 ± 0.50) nm. At the highest annealing temperature shown in Fig. 2(e), the nucleation density has decreased relative to that in Fig. 2(d) and the rms roughness has decreased to (11.34 ± 0.28) nm. Evidence for significant crystallite nucleation and the associated increase in roughness are observed at roughly halfway across the sample. Based on these images, the measured values for roughness range from 0.5 to 13.0 nm, shown in Fig. 3. This range of values can be reproduced regularly using the described preparation conditions.

We postulate that the variation in substrate characteristics is purely topological and that variations in surface energy due to chain packing are minimal. Although contact angle measurements on roughened surfaces can be complicated by pinning of the contact line [15], we have measured the water contact angle across the crystallinity gradient, and found it to be essentially constant at $75.4° \pm 3.4°$, consistent with the results of Park and Griffith who found no statistically significant difference in the surface energy of amorphous and crystalline PLLA [7].

3.2. Measurements of cell proliferation

Cell proliferation was investigated using osteoblastic MC3T3-E1 cells, which were cultured for 1, 3 or 5 d and counted using automated fluorescence microscopy. In Fig. 4 is shown a plot of cell number as a function of position, with each data point representing an average over six samples using three different cell populations. The rate of proliferation appears to be inversely correlated with the surface roughness and shows a relatively steady decrease with increasing roughness. A decrease in rate of proliferation after 5 d at position 1 is attributed to inadvertent collection of isolated data beyond the edge of the PLLA film. It appeared that cell division seemed to occur most rapidly when clusters of cells were formed. This lead to larger variations in cell counts at 5 d because cells on local regions of the film were approaching confluency.

In Fig. 5 is shown a montage of AFM and fluorescence microscopy images that represent the observed trends. The results between individual experiments compared favorably with each other, although there would occasionally be regions in the library with significantly more or less cells than observed on the other gradients. The sharpest increase in roughness occurs toward the crystalline end of the library where the nucleation density and polymer mobility were optimal for crystallization and it might be expected that the proliferation behavior should have a similar step-function appearance. However, the trend toward decreasing proliferation with increasing roughness is unambiguous.

In Fig. 6 is shown a plot of cell number at 3 d as a function of rms roughness. To analyze these data, the Bonferroni method of the Student t-test at ($p < 0.05$) [16] was used to compare the proliferation results at each library position with those measured on the smoothest region of the library. The data from lowest levels of roughness have a composite roughness of (0.54 ± 0.17) nm to which the proliferation data at increasing roughness values were compared. The critical roughness, where a statistically significant decrease in the average number of cells measured at 3 d is observed, occurs at (1.05 ± 0.21) nm in regions with topographic features of approximately 5 nm. The registry between the roughness measurements, taken over domains of 20 μm, and the proliferation measurements, taken over domains of 1500 μm, is not perfect but the transition to lower rates of proliferation in the region displaying incipient nucleation was constant. The proliferation data at the highest roughness values do not show a clear trend. This suggests that rms roughness may not be the correct dependent variable. As it is calculated, rms

Fig. 2. Representative AFM images showing the evolution of crystalline morphology. (a) Image of the completely amorphous region with a nominal annealing temperature of 45°C and an rms roughness of (0.54 ± 0.17) nm. (b) Image of gradient region annealed at a nominal temperature of 60°C. Evidence for incipient nucleation is observed, suggesting some pre-crystallization events occurred. The topographic feature heights are approximately 5 nm leading to an rms roughness of (1.05 ± 0.21) nm. (c) Image of gradient region annealed at a nominal temperature of 70°C having a measured rms roughness of (3.84 ± 0.92) nm. Distinct nuclei are observed and some crystallization has occurred. (d) Image of region of film that was annealed at 85°C. The measured nucleation density is maximal in this region, leading to poorly form crystallites and an rms roughness of (13.00 ± 0.50) nm. (e) Completely crystallized region of film annealed at a nominal temperature of 100°C. The nucleation density appears to be lower than in image (d) and the crystallites more clearly resolved. The rms roughness is (11.34 ± 0.28) nm and the maximum feature height is approximately 40 nm. The standard uncertainty is denoted by the error bars, which represent the standard deviation over three measurements.

(a)

X   5.000 μM/ div
z   20.000 nM / diu

(b)

X   5.000 μM/ div
z   20.000 nM / diu

(c)

X   5.000 μM/ div
z   50.000 nM / diu

(d)

X   5.000 μM/ div
z   50.000 nM / diu

(e)

X   5.000 μM/ div
z   50.000 nM / diu
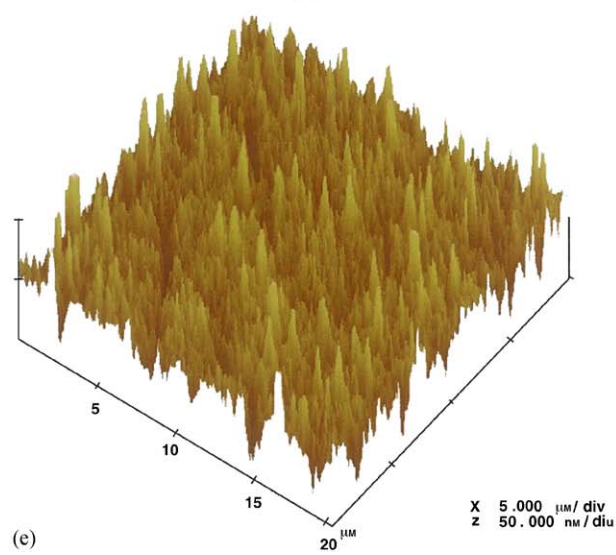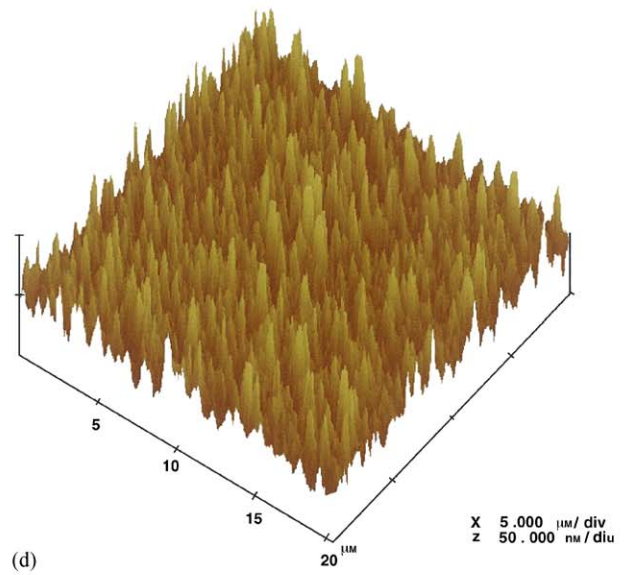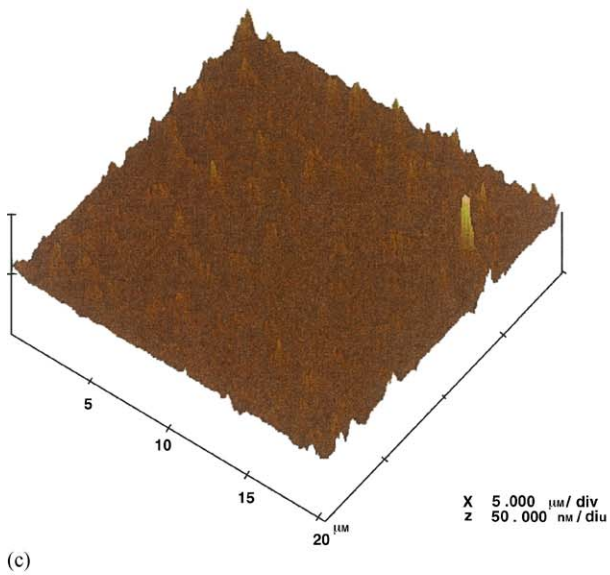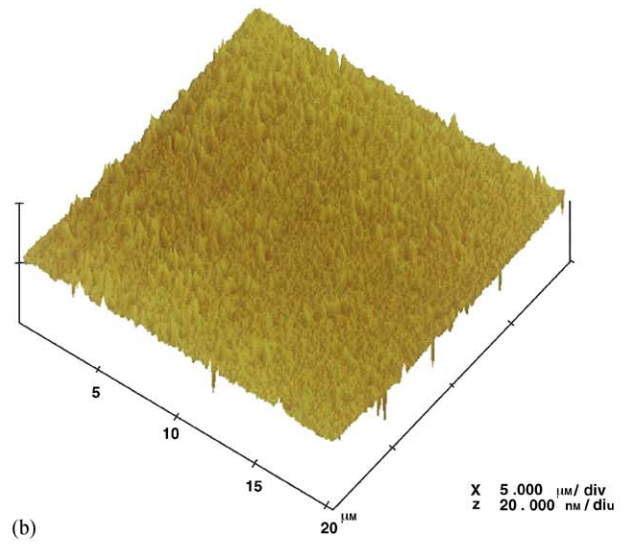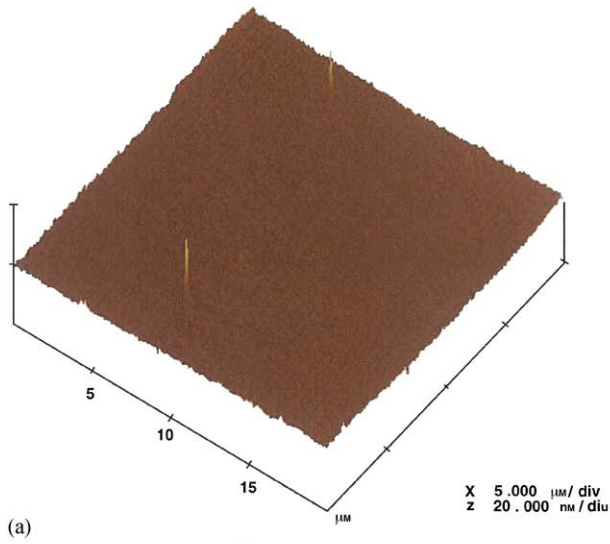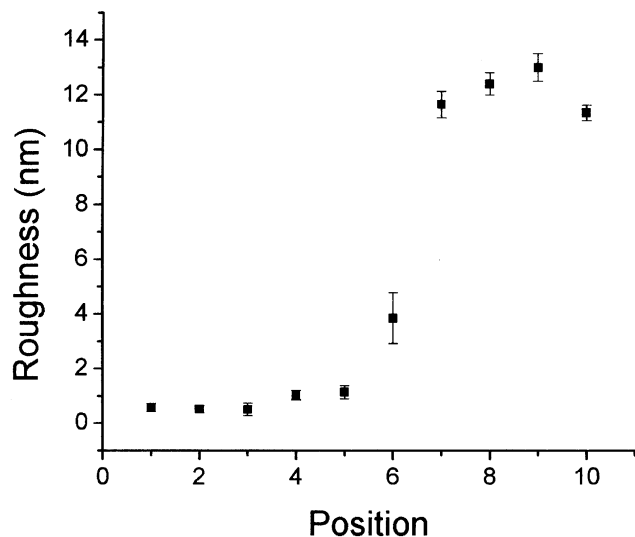
Fig. 3. Plot of average measured roughness as a function of library position. The standard uncertainty is denoted by the error bars, which represent the standard deviation over three measurements.
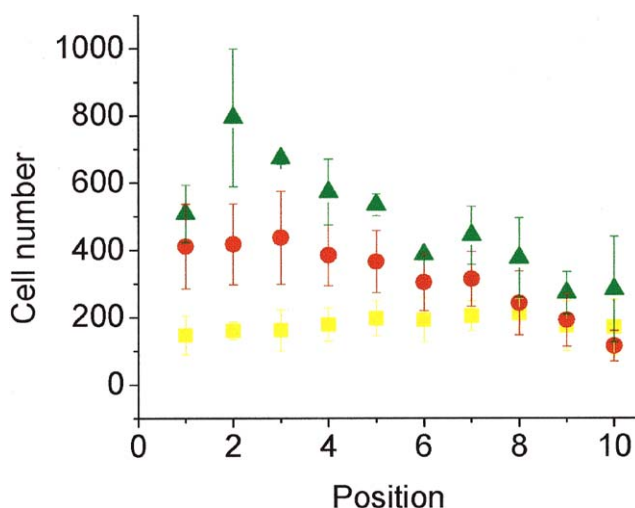
Fig. 4. Plot of average cell number as a function of library position after culturing for 1, 3 and 5 d. Each data point represents measurements on six samples where counts at each library position were performed in 10 regions of constant degree of crystallinity. The standard uncertainty is denoted by the error bars, which represent the standard deviation over multiple measurements.

roughness does not account for the lateral distribution of topographic features, which other researchers have suggested is crucial for determining cellular response [2].

3.3. Mechanisms of effect

Changes in surface properties that effect changes in adherent proteins are known to have strong influences on the behavior of MC3T3-E1 cells [17]. One possible mechanism for the effect of nanometer-scale roughness is to influence the concentration or conformation of

adherent serum proteins, which might be understandable given the comparable sizes of the surface topography and the proteins. It is known that cells reorganize these adherent proteins in a process that is necessary for proliferation [18], and nanometer-scale roughness has been implicated in the measurement of strongly adhering proteins on dialysis membranes [19]. MC3T3-E1 cells have been shown to adhere to fibronectin and vitronectin-coated surfaces [20], using, among others, the $\alpha_5 \beta_1$ integrin to bind to fibronectin in standard culture conditions [17,21]. To investigate this we performed ELISA experiments on homogeneous smooth and crystalline substrates. The first experiment used a model system of human fibronectin without any other serum proteins and measured adhesion of the monoclonal antibody that targets the cell-binding domain of this extracellular matrix protein [12]. The absorbance values measured in this experiment were $(5.6 \pm 0.6) \times 10^4$ and $(6.5 \pm 0.2) \times 10^4$ for the smooth and crystalline PLLA, respectively. The second experiment used a monoclonal antibody for human vitronectin, for which we found good cross-species reactivity with the bovine vitronectin in our culture medium. The absorbance values measured in this experiment were $(5.0 \pm 0.5) \times 10^3$ and $(4.5 \pm 1.7) \times 10^3$ for smooth and crystalline PLLA, respectively. Both these experiments suggest that a minor increase in the amount of adsorbed attachment proteins might occur on the crystalline substrate but not one large enough to generate significant effects on cell proliferation.

While there does not appear to be significant changes in the serum proteins adsorbed to the gradient library, we investigated whether systematic differences in the number, morphology, or distribution of adhesive structures are formed on different regions of the library. Cell division can be affected by integrin-mediated signaling, which involves the formation of adhesive complexes such as focal adhesions [22]. Receptor clustering has been implicated as an initial step in the proliferative response to both extracellular matrix proteins [18] and growth factors [23]. We stained for paxillin, a cytoplasmic protein that localizes to focal adhesions [24], and representative fluorescence images of the cells are shown in Figs. 7(a)–(c). Fig. 7(a) is on the smoothest region of the library, Fig. 7(b) on a region of intermediate crystallinity, and Fig. 7(c) was taken on the fully crystalline region of the film. The focal adhesions tend to localize at the periphery of the membrane on the advancing edges of the cell. No significant differences in the size of the adhesions or their distribution was observed, suggesting that the mechanism for inhibiting proliferation is not dependent on the mode of cellular adhesion.

Cell area has been shown to be a marker for changes in rates of proliferation, and Dalby et al. [25] observed systematic changes in fibroblast morphology
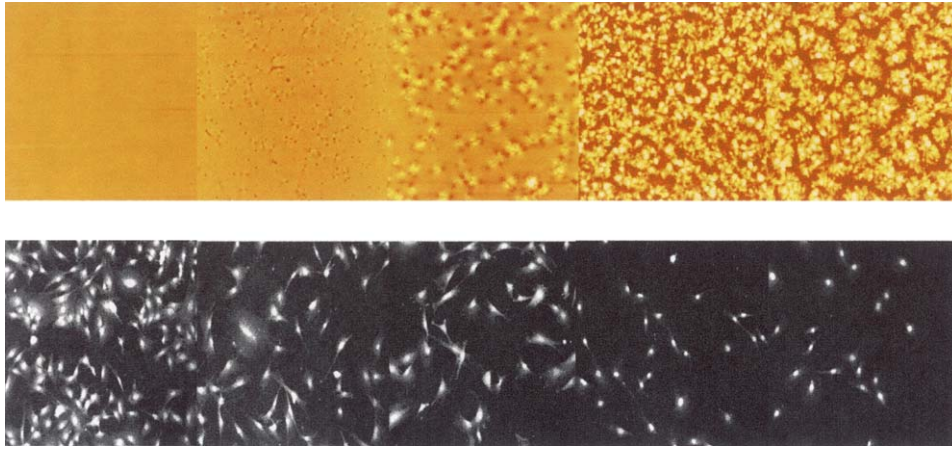
Fig. 5. Montage of representative images of PLLA morphology from AFM data (top panels, field of view in each image is 20 μm), and corresponding cell count from fluorescent microscopy (bottom panels, field of view in each image is 1500 μm).
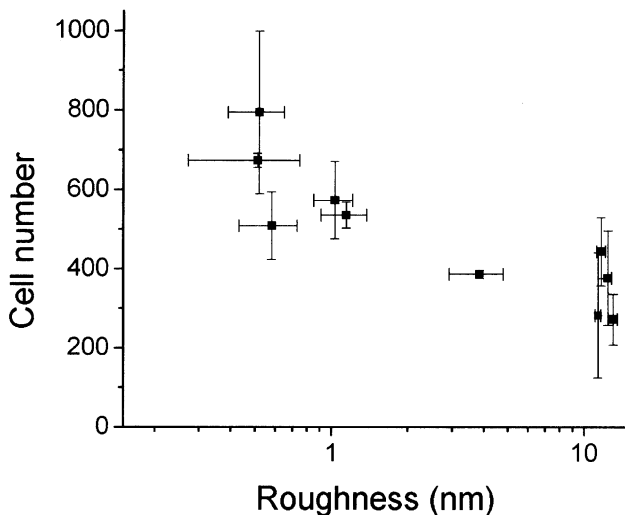
Fig. 6. Plot of cell number as a function of substrate roughness after culturing for 3 d. Using the Bonferroni method for the *t*-test at ($p < 0.05$), the roughness value where a statistically significant decrease in cell number occurs, as compared to the cluster of measurements taken at the lowest three roughness values, is at (1.00 ± 0.17) nm. This corresponds to the region of the gradient library where incipient nucleation occurred, which lead to feature heights of approximately 5 nm. The standard uncertainty is denoted by the error bars, which represent the standard deviation over multiple measurements.

on phase-separated polymer blends having topographic features ranging from 1 to 95 nm that led to variations in cell shape and F-actin organization. Using AFM, we quantified the average area per cell across the gradient libraries after culturing for 1 d and the results are shown in Fig. 8. No systematic trend is observed across the sample, suggesting the changes in proliferation on these samples are decoupled from cell shape.

Changes in the cytoskeleton have also been implicated in regulating cell proliferation [26], and Dalby et al. [25] established correlations on the phase-separated polymer blends they investigated. Compared with the control substrates having roughness values of approximately 1 nm, cells on the substrates having 13 nm roughness displayed greater spreading, higher degrees of F-actin organization, and an increased fraction of cells in S-phase, suggesting that a link exists between nanometer-scale topography, cytoskeleton organization, and proliferation [25]. Using phalloidin staining of F-actin we investigated whether such a relationship exists in the cellular response to our samples where the roughness ranges up to 13 nm. In Fig. 9(a) is shown a representative cell on the smooth part of the library, in Fig. 9(b) is shown an image from a region with intermediate crystallinity, and in Fig. 9(c) is shown one on the fully crystalline part. It was noted that cells had more polygonal processes on the crystalline substrate, which might be conforming to the underlying substrate, but there did not appear to be any significant variation in the amount or distribution of actin filaments. This was confirmed across the entire library by performing quantitative fluorescence microscopy. The background-corrected integrated intensity per cell for each column in the library is shown in Fig. 10 and is seen to be essentially flat, suggesting that indeed there is no significant variation in amount of F-actin as a function of substrate crystallinity. In contrast to the crystallinity libraries, Dalby et al. [25] observed an increase in cell area and proliferation when comparing the results of the featureless control surfaces and the surface with 13 nm features, whereas our results suggest a significant decrease in proliferation occurs. The reason for the fundamental discrepancy between crystallinity gradients and the phase-separated blend of Dalby et al. is unclear. It should be noted that samples prepared in our labs having rms roughness values up to 40 nm did appear to negatively impact actin polymerization and
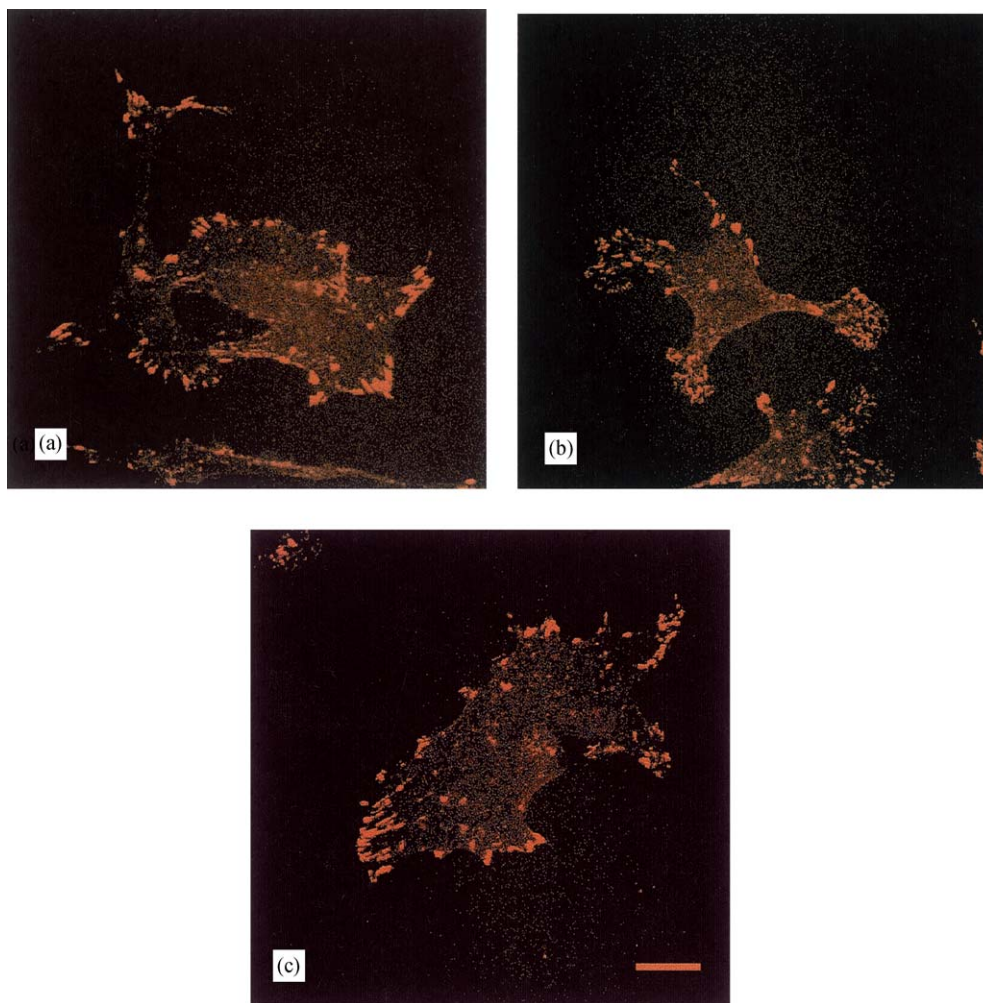
Fig. 7. Fluorescence microscopy images of anti-paxillin-stained cells on: (a) amorphous PLLA, (b) PLLA with intermediate crystallinity, and (c) fully crystalline PLLA. No significant variation in the number, position or shape of the adhesion plaques were observed across the library. Bar at lower right in panel (c) represents 20 μm.
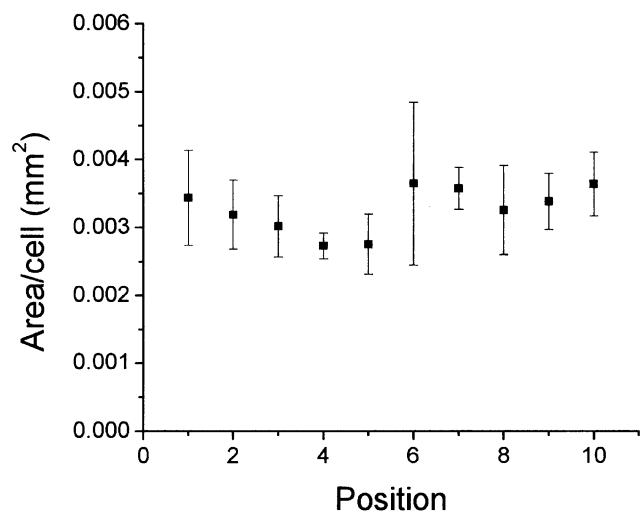
Fig. 8. Plot of area/cell as a function of library position. The standard uncertainty is denoted by the error bars, which represent the standard deviation over multiple measurements. No systematic trend in area per cell was observed through visual inspection of the images.

cell area (data not shown), but observation of these markers does not appear to be necessary for the retardation of proliferation. The contrast between our results and those of Dalby et al. suggests that the spatial organization of nanometer-scale topographic features is capable of positively or negatively regulating mitosis.

4. Conclusions

Using a novel high-throughput method for creating gradients in polymer crystallinity, we have demonstrated that cells are exquisitely sensitive to variations in nanometer-scale topography. Our results indicate that cells are sensitive to topographic features on the order of 5 nm and that the observed inhibition of proliferation does not appear to be mediated through changes in adherent proteins but rather appears to be directly due to changes in substrate roughness. While correlations
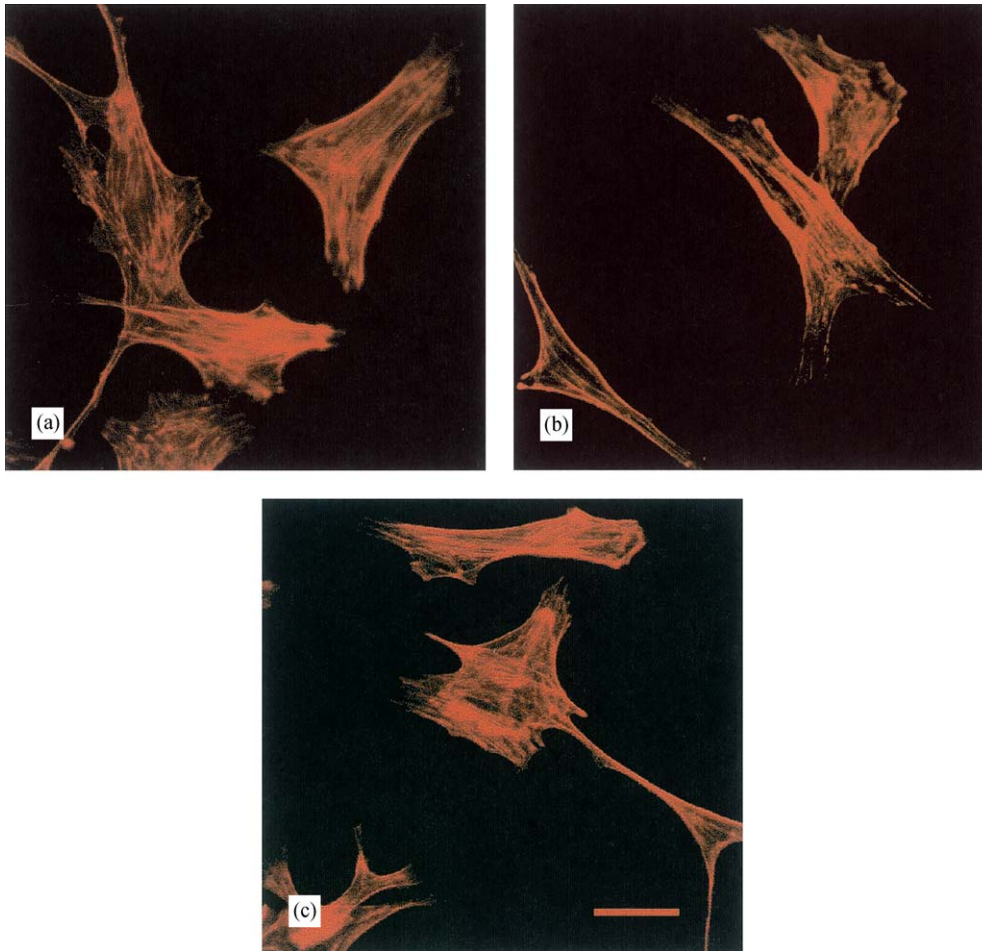
Fig. 9. Representative fluorescence images of phalloidin-stained cells after culturing for 1 d on (a) amorphous, (b) intermediate, and (c) crystalline PLLA. Extensive F-actin networks are observed in each case and no significant variation in cell area is visible although there might be a tendency toward the formation of polygonal processes on the fully crystallized substrates, which appear to correspond with the morphological features observed in these films. Bar at lower right in panel (c) represents 20 μm.
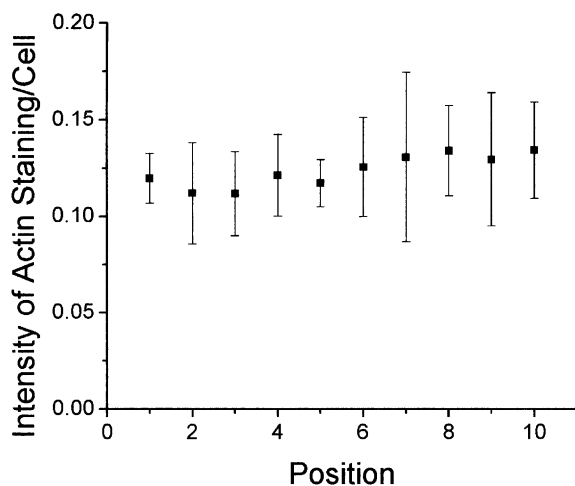
Fig. 10. Integrated intensity/cell for phalloidin-stained cells. Images were background-corrected, and the total intensity from the fluorescence channel was divided by the number of nuclei counted in each frame. The standard uncertainty is denoted by the error bars, which represent the standard deviation over multiple measurements.

between nanometer-scale roughness, actin polymerization, and proliferation have been shown in other systems, our results suggest that cells are much more sensitive to topography than previously expected, and the inhibition of proliferation may be mediated through other mechanisms. The down-regulation of cell division on crystalline surfaces compared with the up-regulation on phase-separated polymer blends [25] suggests that the details of topographic organization are capable of exerting both positive and negative influences on proliferation.

Acknowledgements

References

[1] Flemming RG, Murphy CJ, Abrams GA, Goodman SL, Nealy PF. Effects of synthetic micro- and nano-structured surfaces on cell behavior. Biomaterials 1999;20:573–88.

[2] Anselme K, Bigerelle M, Noel B, Iost A, Hardouin P. Effect of grooved titanium substratum on human osteoblastic cell growth. J Biomed Mater Res 2002;60:529–40.

[3] Lincks J, Boyan BD, Blanchard CR, Lohmann CH, Liu Y, Cochran DL, Dean DD, Schwartz Z. Response of MG63 osteoblast-like cells to titanium and titanium alloy is dependent on surface roughness and composition. Biomaterials 1998;19: 2219–32.

[4] Pins GD, Toner M, Morgan JR. Microfabrication of an analog of the basal lamina: biocompatible membranes with complex topographies. FASEB J 2000;14:593–602.

[5] Wang D, Christensen K, Chawla K, Xiao G, Krebsbach PH, Franceschi RT. Isolation and characterization of MC3T3-E1 preosteoblast subclones with distinct in vitro and in vivo differentiation/mineralization potential. J Bone Miner Res 1999; 14:893–903.

[6] Meredith JC, Sormana J-L, Keselowsky BG, Tona A, Karim A, Amis EJ. Combinatorial characterization of cell interactions with polymer surfaces. J Biomed Mater Res 2003;66:483–90.

[7] Park A, Griffith LG. In vitro cell response to differences in poly-L-lactide crystallinity. J Biomed Mater Res 1996;31:117–30.

[8] Mikos AG, Sarakinos G, Lyman MD, Ingber DE, Vacanti JP, Langer R. Prevascularization of porous biodegradable polymers. Biotechnol Bioeng 1993;42:716–23.

[9] Meredith JC, Smith AP, Karim A, Amis EJ. Combinatorial materials science for polymer thin-film dewetting. Macromolecules 2000;33:9747–56.

[10] Beers KL, Douglas JF, Amis EJ, Karim A. Combinatorial measurement of crystallization growth rate and morphology in thin films of isotactic polystyrene. Langmuir 2003;19:3935–40.

[11] Attawia MA, Uhrich KE, Botchwey E, Langer R, Laurencin CT. In vitro bone biocompatibility of poly(anhydride-co-imides) containing pyromellitylimidoalanine. J Orthopaed Res 1996;14: 445–54.

[12] Schoen RC, Bentley KL, Klebe RJ. Monoclonal antibody against human fibronectin which inhibits cell attachment. Hybridoma 1982;1:99–108.

[13] Wunderlich B. Macromolecular physics: crystal nucleation, growth, annealing. New York: Academic Press; 1976, p. 461.

[14] Lu L, Mikos AG. Poly(lactic acid). In: Mark JE, editor. Polymer data handbook. Oxford: Oxford University Press; 1999. p. 627–33.

[15] Joanny JF, de Gennes PG. A model for contact angle hysteresis. J Chem Phys 1984;81:552–62.

[16] Miller RG. Simultaneous statistical inference. New York: Springer; 1981, p. 299.

[17] Stephanson SN, Byers BA, Garcia AJ. Enhanced expression of the osteoblastic phenotype on substrates that modulate fibronectin and integrin receptor binding. Biomaterials 2002;23:2527–34.

[18] Altankov G, Grinnell F, Groth T. Studies on the biocompatibility of materials: fibroblast reorganization of substratum-bound fibronectin on surfaces varying in wettability. J Biomed Mater Res 1996;30:385–91.

[19] Conti M, Donati G, Cianciolo G, Stefoni S, Samori B. Force spectroscopy study of the adhesion of plasma proteins to the surface of a dialysis membrane: role of the nanoscale surface hydrophobicity and topography. J Biomed Mater Res 2002; 61:370–9.

[20] Sommerfeldt DW, McLeod KJ, Rubin CT, Hadjiargyrou M. Differential phosphorylation of paxillin in response to surface-bound serum proteins during early osteoblast adhesion. Biochem Biophys Res Commun 2001;285:355–63.

[21] Moursi AM, Globus RK, Damsky CH. Interactions between integrin receptors and fibronectin are required for calvarial osteoblast differentiation in vitro. J Cell Sci 1997;110: 2187–96.

[22] Howe A, Aplin AE, Alahari SK, Juliano RL. Integrin signaling and cell growth control. Curr Opin Cell Biol 1998;10: 220–31.

[23] Moro L, Dolce L, Cabodi S, Bergatto E, Erba EB, Smeriglio M, Turco E, Retta SF, Giuffrida MG, Venturino M, Godovac-Zimmerman J, Conti A, Schaefer E, Beguinot L, Tacchetti C, Gaggini P, Silengo L, Tarone G, Defilippi P. Integrin-induced epidermal growth factor (EGF) receptor activation requires c-Src and p130Cas and leads to phosphorylation of specific EGF receptor tyrosines. J Biol Chem 2002;277:9405–14.

[24] Turner CE. Paxillin. Int J Biochem Cell Biol 1998;30:955–9.

[25] Dalby MJ, Riehle MO, Johnstone HJH, Affrossman S, Curtis ASG. Polymer-demixed nanotopography: control of fibroblast spreading and proliferation. Tissue Eng 2002;8:1009–108.

[26] McCabe LR, Last TJ, Lynch M, Lian J, Stein J, Stein G. Expression of cell growth and bone phenotypic genes during the cell cycle of normal diploid osteoblasts and osteosarcoma cells. J Cell Biochem 1994;56:274–82.